

POD analysis of crosswind forces on a tall building with square and H-shaped cross sections

L. Cheng, K.M. Lam* and S.Y. Wong

Department of Civil Engineering, The University of Hong Kong, Pokfulam Road, Hong Kong

(Received December 19, 2014, Revised April 9, 2015, Accepted April 23, 2015)

Abstract. The shape of a tall building has significant impact on wind force generation and wind-induced dynamic response. To study the effect of recessed cavities, wind excitations on a wind-tunnel model of an H-section tall building were compared with those on a square-section building model. Characteristics of the fluctuating wind pressures on the side faces of the two tall buildings and their role in the generation of crosswind forces on the buildings were investigated with the space-time statistical tool of proper orthogonal decomposition (POD). This paper also compares the use of different pressure data sets for POD analysis in situations where pressures on two different surfaces are responsible for the generation of a wind force. The first POD mode is found to dominate the generation of crosswind excitation on the buildings.

Keywords: tall buildings; wind pressure; crosswind excitation; POD

1. Introduction

Buildings with a high height-to-breath aspect ratio are susceptible to mildly aeroelastic behavior due to dynamic wind actions. The fluctuating wind pressures on the building surfaces are mainly caused by a number of mechanisms including the natural turbulence in the incident wind flow, and the unsteady flow behavior generated by the bluff building structure itself in the form of flow separation, reattachment or vortex shedding. Acting on the building surface, the fluctuating wind pressures generate dynamic wind loads which are usually resolved into the along-wind, crosswind and torsional directions. This division of dynamic wind actions in along-wind forces, crosswind forces and torsional moments is not only for the geometry of the wind axes but also from different generation mechanisms of fluctuating wind pressure and forces. For a very flexible aeroelastic building, additional fluctuating forces are induced by the movement of the building itself (Holmes 2015).

For a tall and slender building, the crosswind and torsional responses are often more critical than the along-wind responses both in terms of limit state design and serviceability. At normal wind incidence where the largest wind actions usually occur, the along-wind response follows the fluctuations of the approaching flow and can be reasonably well predicted by the ‘gust factor approach’ based on quasi-static theory. The crosswind response is influenced by the fluctuations of the shear layers and possible vortex shedding from the building. It is more difficult to describe or

*Corresponding author, Associate Professor, E-mail: kmlam@hku.hk

predict the crosswind actions and response with simple generalizations. This is a reason why most current wind codes mainly cover the estimation of along-wind responses but not the crosswind and torsion responses except for buildings of very simple geometries.

There have been few studies focusing on the detail space-time characteristics of the fluctuating wind pressures on a building and the generation mechanisms of crosswind or along-wind actions from the fluctuating pressure. With the availability of the simultaneous multi-port pressure scanning technique, a few recent works attempted to address these questions. Bartoli and Ricciardelli (2010) measured simultaneous wind pressure signals on all faces of a medium-rise rectangular plan building. It is found that the characteristics of pressure fluctuations on the leeward and side faces are rather different from those on the windward faces. The study reinforces that the non-validity of the quasi-steady approach to the velocity-pressure effect on these building faces. Carassale and Brunenghi (2011) applied a number of statistical analyses to the pressure data obtained on a tall building model with multi-port pressure scanning. Some fundamental characteristics of pressure fluctuations on the building side walls leading to crosswind forces were explored with statistical tools such as principal component analysis and independent component analysis. It is evident from these studies that more fundamental investigations on of the space, time, amplitude characteristics of building pressure fluctuations is required for a full understanding of the generation of dynamic wind forces on a tall building.

On the other hand, there have been many studies aiming at a possible mitigation or modification of the crucial crosswind actions and excitation on a tall building. Small aerodynamic treatments of the building cross-section, such as chamfering corners and corner cuts have been shown to be effective in reducing the crosswind response of tall buildings with near-square sections (e.g., Kwok 1988, Tse *et al.* 2009). Other methods, such as tapering of building sections and provision of through-building openings have also been tested (e.g., Kim and Kanda 2010, Dutton and Isyumov 1990, To *et al.* 2012).

The present authors have studied the effect of recessed cavities on the dynamic wind loads of a square tall building (Wong and Lam 2013). Recessed cavities are usually provided in residential tall buildings for ventilation to various services such as bathrooms and kitchens. While there were studies focusing on wind-induced ventilation of these cavities (e.g., Cheng *et al.* 2011), their effect on wind loading behavior had been rarely studied. The previous work of the present authors found that at normal wind incidence on the building face with a cavity, the crosswind excitations and responses of an H-section tall building are significantly reduced from the square-section case. The main set of findings was obtained by the high-frequency force-balance measurements on a series of H-section tall buildings (Wong and Lam 2013). To further investigate the mechanism of wind excitation reduction, fluctuating wind forces acting on different building faces were measured with multi-point pressure scanning and pressure scanning on some selected H-section tall buildings. A correlation analysis of the building face forces suggested that the crosswind forces contributed by the faces of the recessed cavities act in a slightly opposite way to the main contribution from the two main building side faces. This served to explain the reduction of cross-wind excitations.

In the previous study, the cross correlation analysis of crosswind forces mainly shows the phase relationship between the contributions from different building faces. The signatures of the fluctuating wind pressures in the space time distribution, which are more fundamental to the generation of wind forces, were not studied. In the present paper, an advanced statistical analysis based on proper orthogonal decomposition (POD) is carried out to identify the physical phenomena embedded in the crosswind excitation reduction by the recessed cavities. The spatial-temporal analysis of POD could not only identify the typical pressure patterns related to

certain physical phenomena, but also reconstruct reduced-order flow models from the experimental data. POD analysis on the fluctuating wind pressures on building faces combined with some other statistical methods, is discussed in this paper for a better and more effective understanding of pressure-force generation mechanism on buildings with recessed cavities. While the standard POD analysis is applied, the present study attempts to explore the role of the most energetic POD modes in the reconstruction of the crosswind forces so as to reveal the wind load generation mechanism. Another emphasis is on the effect of recessed cavities on the space-time characteristics of fluctuating wind pressures on the building side faces.

2. Wind tunnel testing

The wind pressure data in the present analysis have been obtained in the experiments described previously by Wong and Lam (2013). The experiments were conducted in a boundary layer wind tunnel with a working section of length 12 m, width 3.0 m and height 1.8 m. Triangular spires and floor roughness elements were used to simulate the natural wind flow over the open sea terrain type. The target geometric scale of wind tunnel testing was 1:300. Fig. 1(a) shows the vertical profiles of mean wind speed and turbulence intensity. The power law exponent of the mean wind speed profile was estimated at 0.1. Turbulent velocity spectra had been measured in the wind tunnel and Fig. 1(b) shows the non-dimensional power spectral density of the longitudinal velocity fluctuations at a height of 200 mm. The value of the integral scales of turbulence which best fitted the von-Karman-Harris spectra was $L_{ux} \approx 0.35$ m in the wind tunnel or 105 m full-scale at the geometric scale of 1:300.

Measurement data on an H-section tall building model and the reference square-section tall building model are used in this study. The building models were $H = 0.6$ m in height and the square cross-section or the envelope of the H-shaped cross-section had dimensions of $0.1 \text{ m} \times 0.1 \text{ m}$. The height-to-breadth aspect ratio was $H/B = 6$. The two recessed cavities on the selected H-section building had width (W) and depth (D) at $W/B = 0.25$ and $D/B = 0.25$. Pressure taps were installed on five vertical levels of each building model, at $z/H = \{0.09, 0.28, 0.5, 0.72, \text{ and } 0.91\}$ above the floor. Fig. 2 illustrates the distributions and arrangements of the pressure taps on each level. The pressure taps were installed at five vertical levels at z (mm) = $\{55, 170, 300, 430, \text{ and } 545\}$ above the floor. Fluctuating wind pressures at all taps on a building model were commuted via flexible tubing to six electronic pressure scanners located below the wind tunnel floor. The tubing for all taps had the same length in order to minimize the tubing response error. Furthermore, the inverse transfer function method was applied for tubing response correction (Irwin *et al.* 1979). Near-simultaneous measurement of pressure fluctuations at all taps was made with a pressure scanning system (PSI Initium) at a sampling rate of 500 Hz per port for 120 s (Wong and Lam 2013).

Analysis was made for the two normal wind incidence cases on the H-section building with this notation. “(Normal) wind incidence A” refers to wind direction normal to the building face without a recessed cavity and the other normal case is wind incidence B (Fig. 2). The present study focuses on crosswind forces which are mainly caused by wind pressures on the two building side faces. For the convenience of description, the two side faces are termed the “left side face” (LSF) and the “right side face” (RSF) as appeared to the incident wind. For wind incidence A, there is a recessed cavity on either LSF or RSF. Wind pressure data used for characterization of the side faces for the generation of crosswind fluctuating forces include those on the building side faces and the walls of the cavities (as marked in Fig. 2). For wind incidence B, there is no recessed cavity on

either LSF or RSF and the crosswind force fluctuations are almost entirely contributed by pressures on these two building side faces. Pressures on the side faces of the windward and leeward recessed cavities also contribute to the crosswind force on the building but it was found in the previous work (Wong and Lam 2013) that their contributions are only a few percentage of the total. This is because pressures on opposite side faces of the cavities rise and fall with a largely in-phase relationship and in addition, there is no dominant quasi-periodicity in their fluctuations. Therefore, the present study focuses on the characterization of fluctuating pressures on only the two building side faces at wind incidence B, and how the presence of recessed cavities on the windward and leeward building walls affects their space-time characteristics.

3. Proper orthogonal decomposition

Wind pressure fluctuations produced by unsteady approaching wind and turbulent near-flow separations on the building exhibit a complex spatial temporal structure. Proper Orthogonal Decomposition (POD), also known as Karhunen-Loeve expansion, is a method to detect a coordinate system which can describe the original random phenomena most efficiently. The idea of POD is based on the least square method. The random space time variable field, such as the wind pressure field in this case, is represented by the modal expansion. The POD modes are statistical representations of the variable data in multiple points at a single time, emphasizing on the probabilistic structures instead of temporal features. It can be used to discover the hidden deterministic structure of the random fluctuations.

The first application of POD to analyze wind pressure fluctuations was reported on a cooling tower (Armitt 1968). The advantages of POD were then recognized by many other researchers. Further applications of POD were conducted to study wind pressures on a bluff body (e.g., Lee 1975, Best and Holmes 1983, Kareem and Cermak 1984). POD has also been used to investigate fluctuating wind pressures on large roofs (e.g., Bienkiewicz and Ham 1993, Bienkiewicz *et al.* 1995, Holmes *et al.* 1997, Lam *et al.* 2011). A review of the application of POD on random wind pressure fields was made in Tamura and Suganuma (1999) which also discussed the precautions and validity of the method. Baker (2010) explored the connection between the POD modes and physical flow phenomena and supported the usefulness of POD analysis in representing the fluctuating pressure field on the surface of a structure. The comprehensive two-part review by Solari *et al.* (2007) and Carassale *et al.* (2007) described the theoretical foundations of POD and discussed some applications and prospects of POD in wind engineering.

As described in Solari *et al.* (2007), POD belongs to a family of modal analysis methods which also include techniques such principal component analysis (PCA) and singular value decomposition. Carassale *et al.* (2007) pointed out that POD can be used in a weak form as the covariance proper transformation (CPT), or in a strong form as the spectral proper transformation (SPT). CPT modes are usually connected with one specific mechanism but SPT modes can be interpreted by various phenomena in different frequency ranges. Among the various analysis methods, the standard form of POD analysis remains the most widely used and perhaps the most mature technique for space-time analysis of turbulent flow quantities. Therefore, POD is used for the present study which focuses on the role of various modes of fluctuating pressures in the generation of crosswind forces on the square- or H-section tall building.

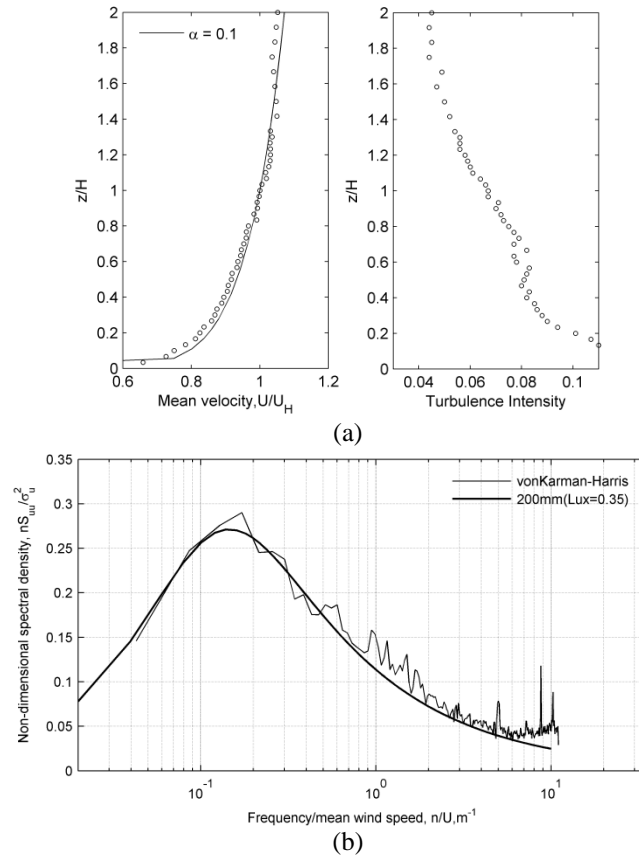


Fig. 1 (a) Mean wind speed profile and turbulence intensity profile and (b) Turbulence spectrum of longitudinal velocity fluctuations, $z = 200$ mm

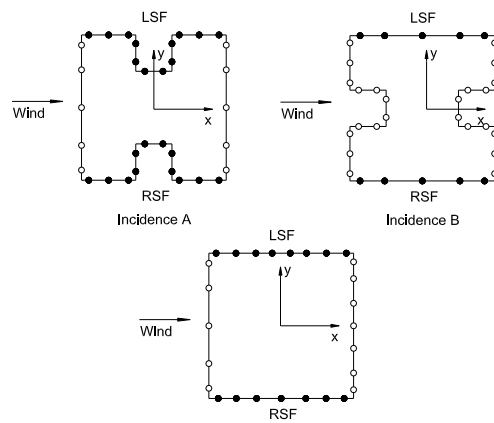


Fig. 2 Distribution of pressure taps on square tall building and H-section tall building. LSF = Left Side Face; RSF = Right Side Face

A major limitation of POD or PCA is the enforcement of orthogonality of its modes which may not be justified from a physical point of view. The technique of independent component analysis (ICA) has been purposed to remedy this restriction and was applied to wind engineering problems (e.g., Carassale and Brunenghi 2011). ICA is analogous to POD but is based on non-orthogonal decomposition. In the application to building pressures, Carassale (2012) demonstrated that ICA may present more recurrent pressure distributions than POD but it needs more strongly correlated modes to compose such pressure distributions. Thus, POD is adopted in this study to illustrate the involvement of the dominant modes in the reconstruction of the crosswind load. Nevertheless, the use of ICA may worth exploring in a future study.

For this paper, POD analysis was carried out for the wind pressure fluctuations on a square-section tall building and an H-section building. The focus is on the characteristics of wind pressures in the generation of crosswind forces. Thus, mainly the pressure signals on the side faces of RSF and LSF were used in the POD analysis (Fig. 2). Three analysis cases were carried out and the results compared. The three cases use different set of pressure signals as listed in Table 1. In Case 1, the space time signals of wind pressures on the two side faces were used to perform the POD analysis but each side face is analyzed separately. In Case 2, the data of the two side faces were combined as one matrix data set which is then subjected to POD analysis. In Case 3, the data matrix was composed of wind pressures on the two side faces, as well as the windward face and the leeward face, that is, all four building faces and all cavity faces.

Before data analysis, all wind pressure signals, at locations \vec{x}_j , were converted into the time histories of pressure coefficients using the mean wind speed at the building roof height as the reference velocity

$$C_p(\vec{x}_j, t) = \frac{p(\vec{x}_j, t)}{\frac{1}{2} \rho \bar{U}_H^2} \quad (1)$$

Pressure coefficients are also used in the subsequent presentation of results. The locations of pressure taps on the present building models were not uniformly distributed (Fig. 2). The effects of non-uniformly distributed pressure taps on the POD analysis were discussed in Jeong *et al.* (2000) in which a correction method, namely the rectangular rule of integration, was proposed for a low rise building. Baker (2000), however, showed that the experimental limitations such as the number of pressure taps and their spatial distribution are more likely to affect the less energetic higher POD modes. In this study, it will be shown that the first few POD modes with high energy contribution already produce good reconstruction of the wind forces. As the higher POD modes are not discussed, the correction for unequal tributary areas was not applied to keep the analysis simple. Therefore, the time histories of wind pressures at the tap locations were directly used as the data sets.

The ‘‘snapshots’’ POD method (Sirovich 1987) has been used in this study, and the procedures are briefly described as follows. Tamura and Suganuma (1999) stated that the POD technique is to find the most efficient axis with most energy in terms of the mean square value and thus the mean value component should be excluded in the calculation of the correlation matrix. Therefore the time-averaged mean pressure coefficients, \bar{C}_p , at all tap locations were computed and removed from the fluctuating pressure field. The spatial-temporal pressure coefficient data is represented by an $M \times N$ matrix, where M is the number of spatial points, that is, pressure taps, and N is the number of time steps in the record (Table 1). Due to the limitation of computation capacity, only the first

1-min. data of the 2-min. measurement time were used for POD analysis. Thus, there were 30,000 time steps and $N = 30,000$. From the data matrix, the spatial correlation matrix was computed and its eigenvalue problem solved as

$$R(\bar{x}_1, \bar{x}_2) = \langle C_p^T(\bar{x}_1, t), C_p(\bar{x}_2, t) \rangle \quad (2)$$

$$R\Phi = \lambda\Phi \quad (3)$$

The N POD modes were obtained as the columns (φ) of the eigen-functions Φ . The corresponding element of the eigenvalue vector λ defines the relative contribution of each mode to the fluctuating pressure field. Thus, the cumulative energy contribution from the first k modes is given by

$$E_k = \sum_{i=1}^k \lambda_i / \sum_{i=1}^N \lambda_i \quad (4)$$

Wind pressure fluctuations of each mode i can be reconstructed as

$$C_{p_i}(\bar{x}, t) = a_i(t)\varphi_i \quad (5)$$

where the coefficients $a_i(t)$ are obtained from the projection of the original data onto the POD modes

$$\mathbf{A} = \langle \Phi^T, C \rangle \quad (6)$$

The reconstruction of pressure data can be made for each mode or a number of modes.

4. Results and discussion

4.1 Distributions of mean and r.m.s. pressure coefficients on side faces

Before presenting the POD results, this section presents the spatial distributions of the simple statistical measures of pressure coefficients on the building faces. Emphasis is on the side faces which contribute to the wind force fluctuations in the crosswind direction. From the pressure coefficient signals in Eq. (1), the mean and root-mean-square (r.m.s.) pressure coefficients were computed. Figs. 3-5 show their distributions on all faces of the square-section tall building and the H-section tall building, respectively. The distributions are expected to be the same on the two side faces and thus the results on one face are presented.

At wind incidence A, it is evident that the distributions of mean and r.m.s. pressure coefficients on the front and rear faces of the H-section tall building share many similarities to those of the square-section tall building in both distribution and magnitudes. On the side faces, the distribution of \bar{C}_p on the H-section building exhibits differences from that of the square-section building due to the existence of the recessed cavities. The presence of a recessed cavity on the side face contributes to a slightly higher negative pressure on the cavity back wall than the respective part of the side face of the reference square building.

Table 1 Pressure data sets for POD analysis

| Case | Pressure data | Spatial point, M | | |
|------|---------------|--------------------|--------------------|-------------|
| | | Square building | H-section building | |
| | | | Incidence A | Incidence B |
| 1 | RSF | 35 | 60 | 25 |
| | LSF | 40 | 60 | 25 |
| 2 | [RSF; LSF] | 75 | 120 | 50 |
| 3 | All Faces | 135 | 170 | 170 |

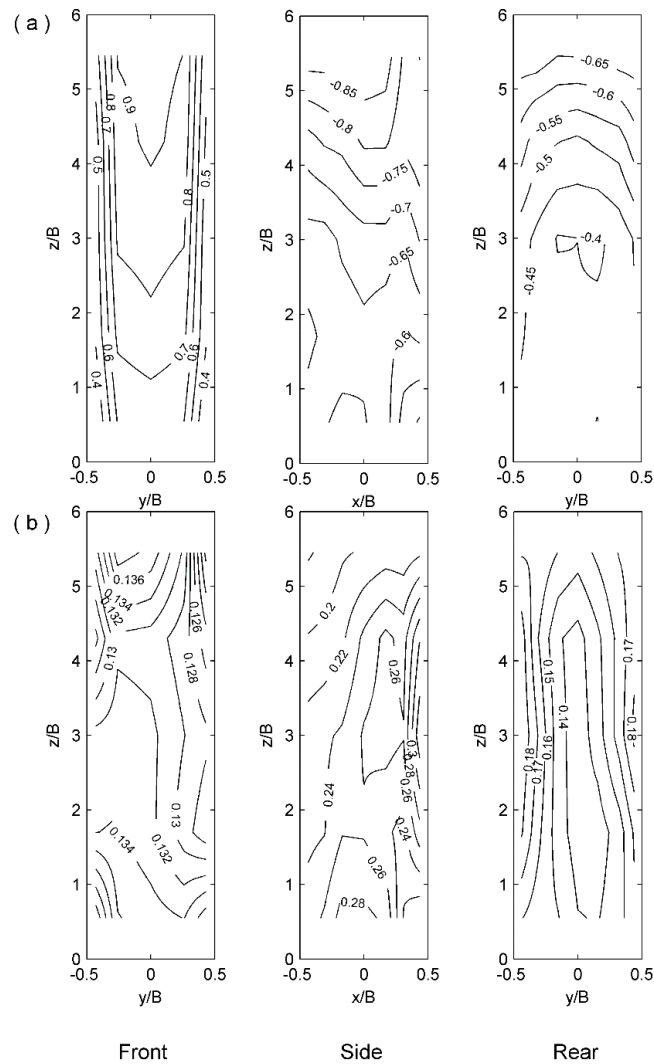


Fig. 3 Distribution of (a) mean and (b) r.m.s. pressure coefficient on all faces of square-section tall building

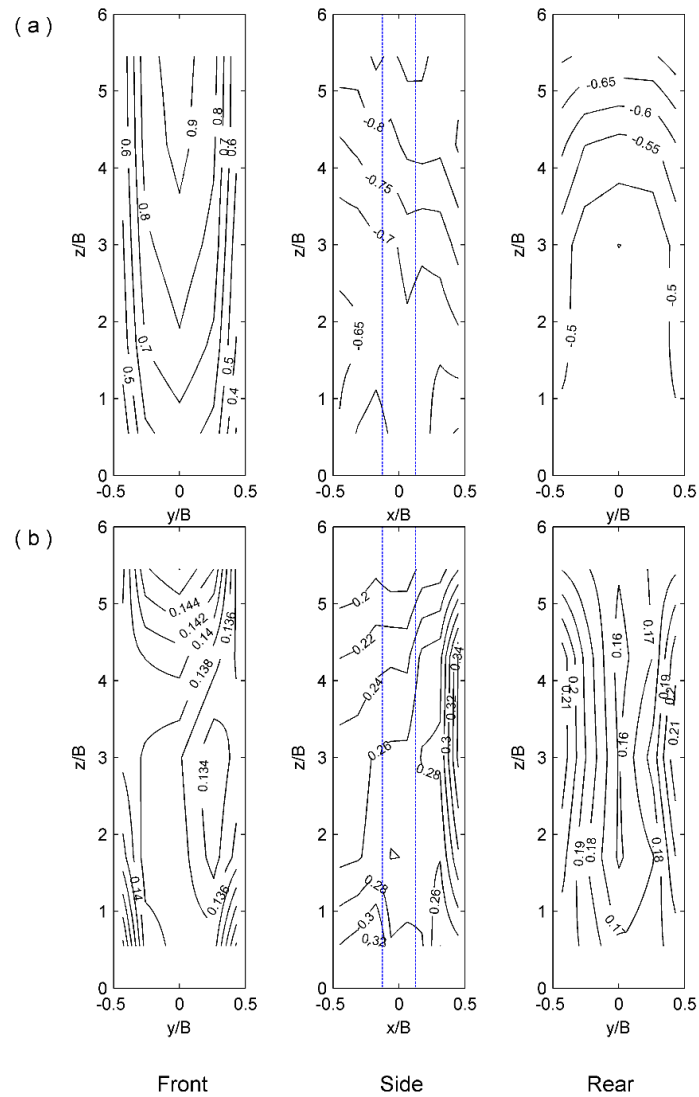


Fig. 4 Distribution of (a) mean and (b) r.m.s. pressure coefficient on all faces of H-section tall building at wind incidence A

Under normal wind incidence B, significant reduction of crosswind excitation was found by Wong and Lam (2013). However, the distributions of mean and r.m.s. pressure coefficients on the two side faces of the H-section building are similar to those of the square tall building. Therefore, higher level statistical analysis is required to explore the underlying flow mechanisms.

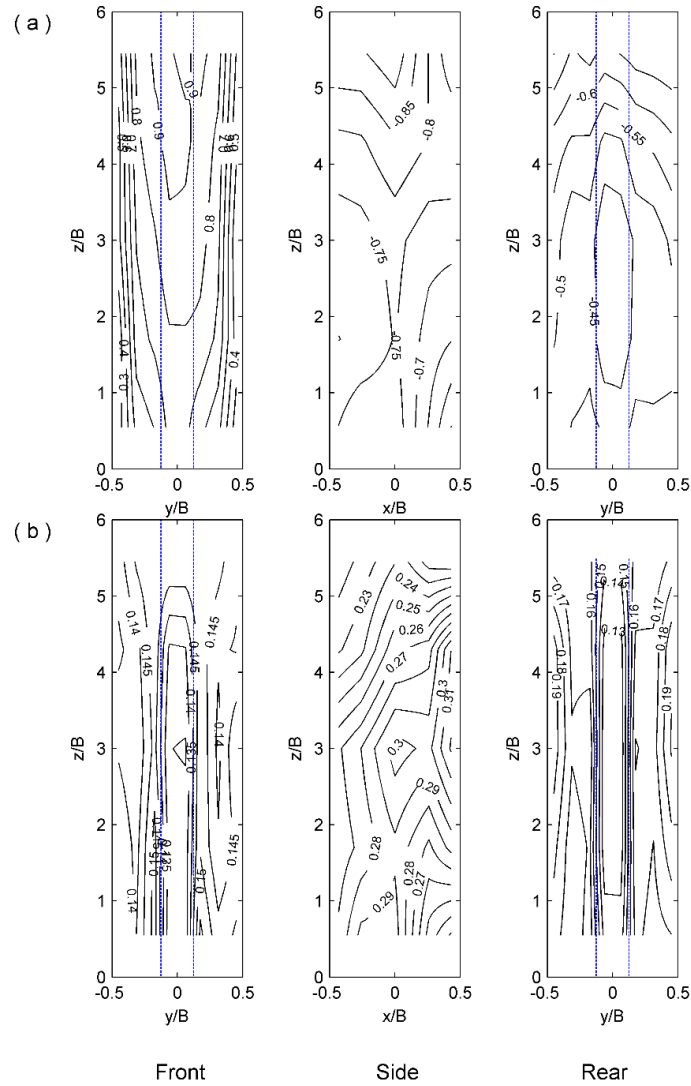


Fig. 5 Distribution of (a) mean and (b) r.m.s. pressure coefficient on all faces of H-section tall building at wind incidence B

4.2 POD modes

POD analysis was applied to the three data sets of pressure coefficients as listed in Table 1. Fig. 6 shows the portion of energy contribution of the first 50 POD modes to the overall energy of fluctuations for the two buildings under the two wind incidence cases. The energy contribution is calculated with Eq. (4). For all data sets, the first 50 modes can represent the complex structure of

wind pressure fluctuations up to over 90% energy. In general, the combination of more complex data sets leads to a less efficient energy convergence. For the POD modes obtained from the wind pressure coefficients on a single side face, the first 10 POD modes contribute more than 90% to the overall energy. For the POD modes consisting of both side faces, more than 10 POD modes are required for inclusion of 90% total energy. When comparing the two building models, insignificant differences are observed in terms of the energy distribution and convergence of the POD modes.

The record of the fluctuating wind pressure field of a given period can be expressed as a trace of the point movement in the pressure space, which is called “state locus” in Tamura and Suganuma (1999). The objective of POD analysis is to find a new mutually orthogonal coordinate system to capture the state locus most efficiently. The wind pressure fields with M pressure measuring points will be expressed as an M -dimension space. The first mode represents the most efficient new coordinate. This could explain why the increase of number of pressure data employed in Cases 2 and 3 of the POD analysis reduce the energy of the first POD mode and slow down the progress of the energy convergence as compared to Case 1.

Figs. 7-9 show the pressure distribution of the first two POD modes on the side faces of the two buildings. In Case 1, wind pressures on RSF and LSF are subjected to POD analysis independently and it is thus expected that the modal amplitudes on the two faces should have the same patterns and magnitudes. However, as observed in Fig. 7, there are inevitably some differences when using experimental wind pressure data. Cases 2 and 3 use the combined data in POD analysis and the resulting POD modes represent the orthogonal patterns of pressures on different building faces which produce a dominant large-scale space-time structure. It is observed in Fig. 7 that the Mode 1 distributions of wind pressure coefficients on RSF and LSF have the same patterns but in the out of phase relationship. The patterns of Mode 2, and many higher modes, on the two side faces are different.

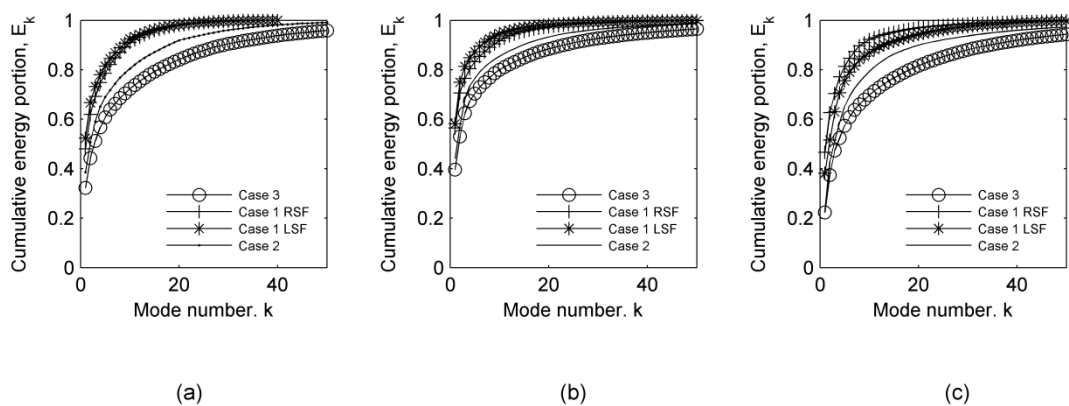


Fig. 6 Cumulative energy contributions of POD modes, (a) Square-section building; (b) H-section building at incidence A; (c) H-section building at incidence B

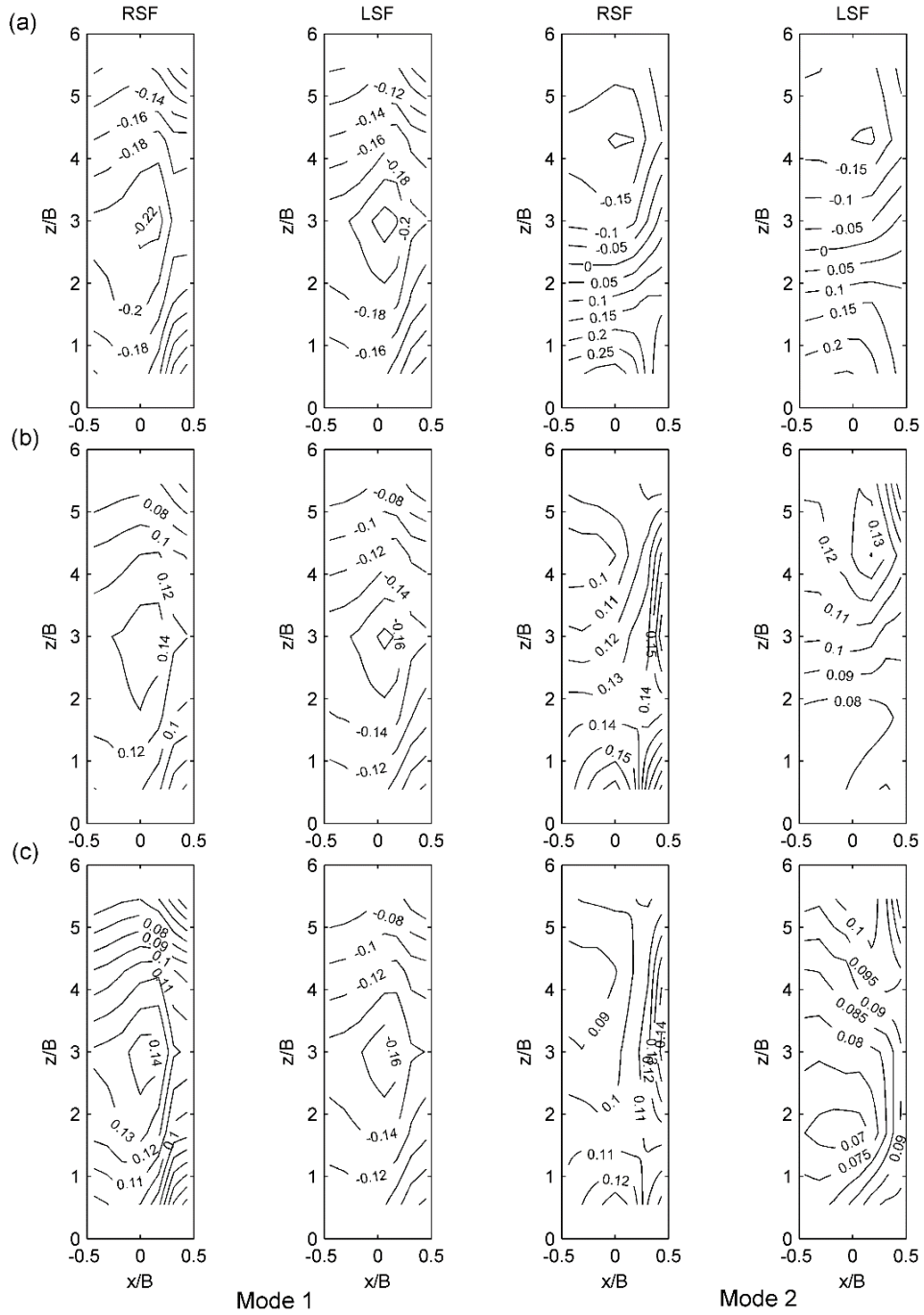


Fig. 7 First two POD modes on side faces of square-section tall building, (a) Case 1; (b) Case 2; (c) Case 3

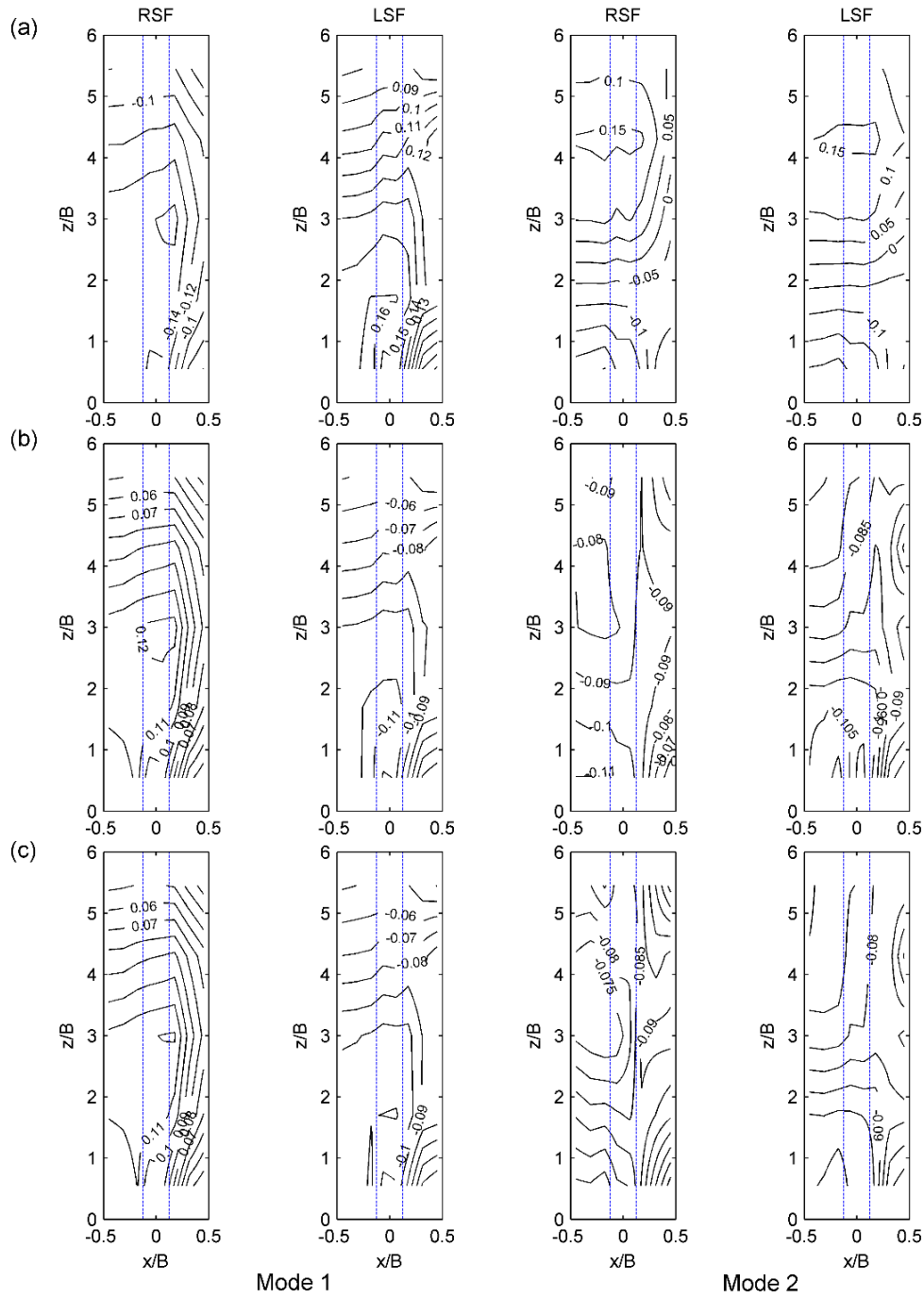


Fig. 8 First two POD modes on side faces of H-section tall building at wind incidence A, (a) Case 1; (b) Case 2; (c) Case 3

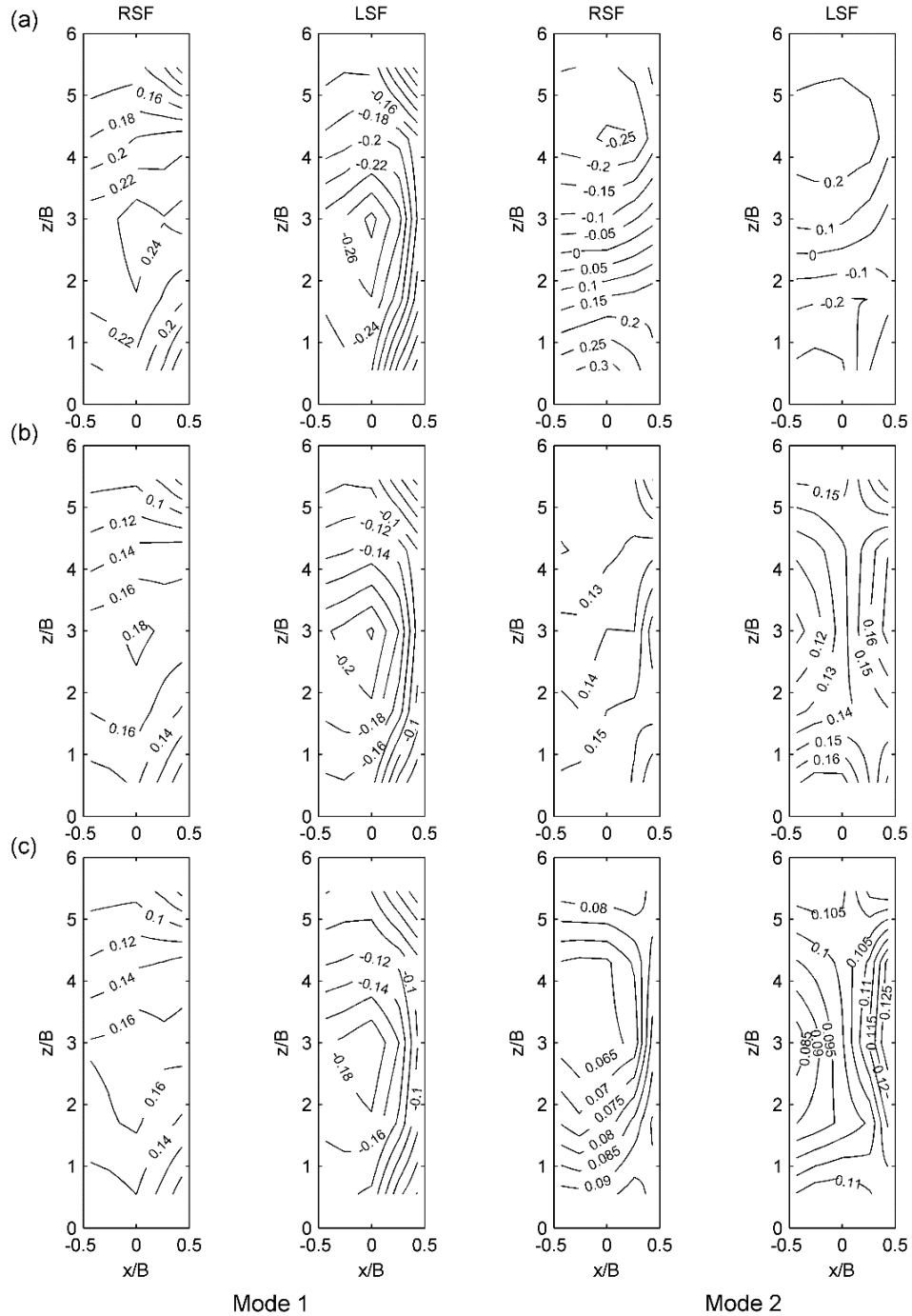


Fig. 9 First two POD modes on side faces of H-section tall building at wind incidence B (a) Case 1; (b) Case 2; (c) Case 3

For the square-section tall building (Fig. 7), all Cases 1-3 give the same patterns for the first POD mode which features pressure fluctuations rising and falling together at all locations on a building side face. The fluctuation amplitudes are largest at the center of the building face and fall in all directions. When the two side faces are considered together, positive pressure fluctuations on one side face are always associated with negative pressure fluctuations of same amplitudes on the other side faces. In this way, they act together to produce coherent Mode 1 crosswind force fluctuations on the building.

In Case 1, Mode 2 patterns exhibit in-phase pressure fluctuations on the upper part of the building face while those on the lower part act with 180° phase difference. Mode 2 patterns in Case 2 and 3 are similar and with wind pressure fluctuations at all locations of both side faces acting in phase. Combined with different modal amplitude patterns on the two faces, mode 2 acts to provide temporal pulsations which weaken the coherent mode 1 crosswind forces. The degree of weakening depends on the combined modal amplitudes on the two side faces. It can be observed in Fig. 7 that the modal amplitudes on the right-side face (RSF) exhibit a narrow ridge along its leeward edge and a small crest near the ground while the remaining larger portion of the building face is in a shallow valley of lower modal amplitudes and with the lowest trough in the upper upwind side of the building face. On the left-side face (LSF), the Mode 2 pattern exhibits a long narrow ridge extending from the upper leeward corner of the face along the leeward edge to the lower leeward corner. The large remaining portion of the face is likewise in a shallow valley but the trough is on the lower windward side of the face. Due to the different topography of Mode 2 amplitudes on the RSF and LSF, the combined effect in weakening the coherent Mode 1 crosswind force fluctuations is small. As a result, the net crosswind force on the square-section building is dominated by the coherent and periodic Mode 1 contribution.

Fig. 8 shows the first two POD modes on the RSF and LSF of the H-section tall building at wind incidence A. The modal amplitudes on the side faces of the recessed cavities do not contribute to the crosswind force on the building and are not shown in Fig. 8. The contour maps in this figure, as well as Figs. 4 and 5, are drawn using the pressure data from the cavity end face and the two parts of a building side face. As such, they cannot reflect the expected discontinuities of values across two different faces so that relevant caution should be made in reading these contours. Compared to Fig. 7, the existence of a recessed cavity on the side face appears to result in reduced magnitude of wind pressure fluctuations in both POD modes in all cases. For Mode 1, the pattern of modal amplitudes also appears to be modified by the presence of recessed cavity. The crest of peak amplitudes on the center of the building side face becomes less distinct from Fig. 7 and it now resides partly inside the cavity back face and partly on the leeward part of the building side face. On the latter surface, the drop of amplitudes towards the leeward edge is steeper. However, the patterns on the RSF and LSF remain grossly the same and with 180° phase difference in Cases 2 and 3. Thus, there is still generation of coherent crosswind force fluctuations from the POD mode 1.

In POD analysis Cases 2 and 3, the modal amplitudes of POD mode 2 in Fig. 8 exhibit similar pattern on RSF as the square-section tall building (Fig. 7) but the distributions on the LSF show very mild variations (that is, nearly constant modal amplitudes over the surface with distinct valleys or crests). The combined effect from the RSF and LSF in weakening the mode 1 crosswind force fluctuations is therefore slightly less than the case of the square-section tall building.

Wind incidence case B is a case for which the crosswind excitation on the H-section building is found significantly reduced from the square-section building situation. Fig. 9 shows that the first POD modes on both building side faces (RSF and LSF) have very similar patterns as the

square-section building case. Coherent and periodic crosswind force fluctuations are likewise produced by pressure fluctuations of this POD mode.

Unlike the first mode showing 180° phase difference between the RSF and LSF, the second POD mode (in Cases 2 and 3) shows in-phase pressure fluctuations on the two side faces. Mode 2 thus has the same weakening effect on the Mode 1 crosswind force generation by introducing time and spatial pulsations of crosswind forces. One evident observation in Fig. 9 is the generally higher modal amplitudes of Mode 2 as compared to Figs. 7 and 8. Another distinct difference is the relatively simple topography of Mode 2 amplitudes over the RSF or LSF. On the RSF, Mode 2 in Case 2 show rather gentle topography, while Case 3 exhibits a single hill with crest near the center of the face. The general distribution in the latter case is actually quite similar to the mode 1 pattern. On the LSF, Cases 2 and 3 show Mode 2 amplitudes generally dropping from a ridge along the leeward edge towards the windward edge. The reduced complexity in spatial variation of POD Mode 2 leads to a more spatially coherent and larger weakening effect on the Mode 1 crosswind excitation.

The POD results in Figs. 7-9 serve to provide a detail mechanism of crosswind excitation reduction at wind incidence B from the space-time variations of pressure fluctuations on the building side faces.

4.3 Reconstructed crosswind force components

Using a number of POD modes, wind pressure fluctuations can be reconstructed at all tap locations. With pressure integration, crosswind forces on a particular side face can be obtained:

$$F_c(t) = \sum_i^{\text{sideface}} p_i(t) A_{c,i} \quad (7)$$

where $A_{c,i}$ is the tributary area of tap i on the side face and with direction of surface perpendicular to the incident with direction. It should be noted that the direction of the tributary area (its unit normal) is set to always pointing to the LSF and thus all crosswind force components are set positive when acting towards that direction. As with pressure, the crosswind force coefficients are used instead of the forces

$$C_F(t) = \frac{F(t)}{\frac{1}{2} \rho \bar{U}_H^2 BH} \quad (8)$$

For the H-section tall building under wind incidence A, the crosswind force component of a side face is contributed by wind pressures on the side face and the back wall of the recessed cavity on that face (Fig. 2).

As shown in the previous section, the first POD mode is strongly related to the generation of crosswind forces by the building side faces. Therefore, only the first POD mode is used in the reconstruction of pressure fluctuations and crosswind force fluctuations. The total force coefficient signal is obtained after adding into the mean force coefficient which is readily computed from the mean wind pressures.

Fig. 10 shows sample portions of the time histories of crosswind force coefficients from the two side faces and their combination. The original time histories obtained from pressure integration of the measured pressure data, and the reconstructed time histories using only the first POD mode are shown for the two building models under the two wind incidence cases. The parts

of the figures, (a) (b) and (c), present the results of square-section building and H-section building at wind incidence A and B, respectively. The total crosswind force coefficient on the entire building is the combined effect of the corresponding force coefficient on the two side faces. These “net” crosswind force coefficients for the three cases are also shown.

It is observed in Case 1 that the reconstructed crosswind force coefficients on either side face coincide almost perfectly to the original force coefficients for both building models. In Cases 2 and 3, the reconstructed crosswind force coefficient on a side face obviously has slightly lower peak value than the original force signals, especially for the H-section tall building. Similar findings have been found in the POD analysis of pressure fluctuations on the two surfaces of a large cantilevered roof (Lam *et al.* 2011). This is because when pressure data on two different surfaces are combined into one data set for POD analysis, all pressures in one POD mode are forced to the same phase relationship (0° or 180°). The resulting POD mode incorporates the pressure patterns on both surfaces and thus the accuracy of one surface is less than the POD mode on that individual surface only. This may also be a reason for the faster energy convergence of the POD modes in Case 1 where POD analysis is conducted on separated data sets (Fig. 6).

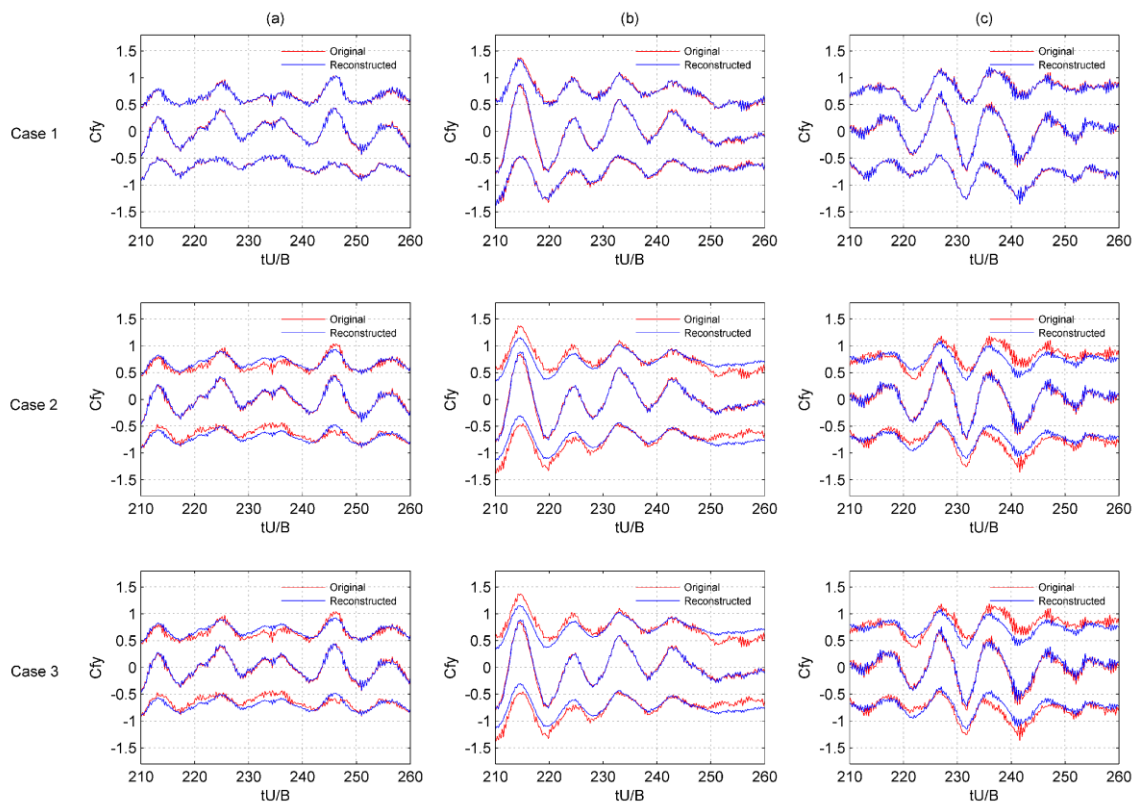


Fig. 10 Time histories of crosswind force coefficients by original signals and reconstructed signals using first POD mode only by Case 1-3 respectively, on: (a) Square-section building; (b) H-section building at incidence A; (c) H-section building at incidence B. In each plot, upper signals are crosswind forces on LSF, lower signals are forces on RSF, and middle signals are net crosswind forces

For the net crosswind force coefficient, however, it is almost perfectly reconstructed using Mode 1 only in all POD analysis cases. The net force is obtained from the combination of pressures on both surfaces and the POD modes in Cases 2 and 3 enforce orthogonality over both surfaces. The observation that the first POD mode in all cases can already well reconstruct the original net crosswind force suggests that the dominant pressure patterns on the two side surfaces producing the net crosswind force largely follow the same phase relationship.

Fig. 11 shows the cross correlation curves between the crosswind force coefficients on the two side faces of both building models. All cross correlation curves exhibit regular quasi-periodicity of crosswind forces at a non-dimensional quasi-period, $\tau\bar{U}_H/B \approx 10$, corresponding to the reciprocal of Strouhal number at 0.1 (Wong and Lam 2013). The peak correlation occurs at zero time lag with a positive value in all cases. This means that the crosswind forces on the two side faces act in the same direction at most times, which is typical for vortex excitation of a slender structure.

For the square tall building, the Mode 1 reconstructed crosswind forces have almost identical cross correlation curves as the original force signals. With the presence of the recessed cavity, either on the windward or side face of the building, the peak correlation value is slightly lower than that for the square tall building. It is also observed that the reconstructed crosswind force signals in Case 1 lead to a further lower peak correlation value at zero time lag. This suggests that the presence of recessed cavities disturbs the dominance of the mode 1 patterns in producing the in-phase relationship between the crosswind forces on the two building side faces.

In Cases 2 and 3 where orthogonality is forced on the two side faces, or with other faces as well, the cross correlation coefficient is always unity at zero time lag. It is noted, however, that while the first troughs of the correlation curves have coefficient values $R < -0.6$ for the square building and the H-section tall building at wind incidence B, the corresponding value has slightly lower magnitude ($R \approx -0.5$) for the H-section tall building at wind incidence A. It is at the latter normal wind incidence case A that the crosswind excitation on a tall building is found to be significantly reduced by the presence of recessed cavity (Wong and Lam 2013). The present result suggests that the reduction is largely reflected in the first POD mode.

To further investigate the correlation relationship between wind excitations from the two side faces, cross power spectral density functions (p.s.d.) of forces on LSF and RSF are computed and shown in Fig. 12. For both building models, the cross spectra of the two original crosswind force components from the two side faces exhibit the peak of vortex excitation at $nB/\bar{U}_H \approx 0.1$, at which the phases are near zero. Across the frequencies, the two side face crosswind force signals reconstructed from POD mode 1 in Case 1 for both buildings show almost identical magnitudes and phases of the cross p.s.d. to those of the original signals, except at some high frequencies.

For the reconstructed force signals in Cases 2 and 3, the phases of the cross p.s.d. are zero at all frequencies, which is expected. The magnitudes of the cross p.s.d. of the reconstructed crosswind forces on the square building model show almost the same magnitudes and distribution as the original signals around the spectral peak of crosswind excitation. This reinforces that the generation of crosswind force on the square tall building can be represented to a very high degree by the first POD mode. For the H-section tall building, however, there are differences in the mode 1 reconstruction both in terms of spectral levels and peak frequency of the spectral peak of the cross p.s.d.

In this section, the contribution of lateral turbulence in the incoming wind flow to the fluctuations in crosswind forces is not explicitly studied. This is partly due to the lack of coherent patterns and structures in the ambient lateral turbulence to be clearly revealed by POD, and partly

due to its likely weak contribution as compared with the contribution from vortex excitation. Nevertheless, the higher modes which are not fully analyzed in this paper may be associated with the lateral wind turbulence.

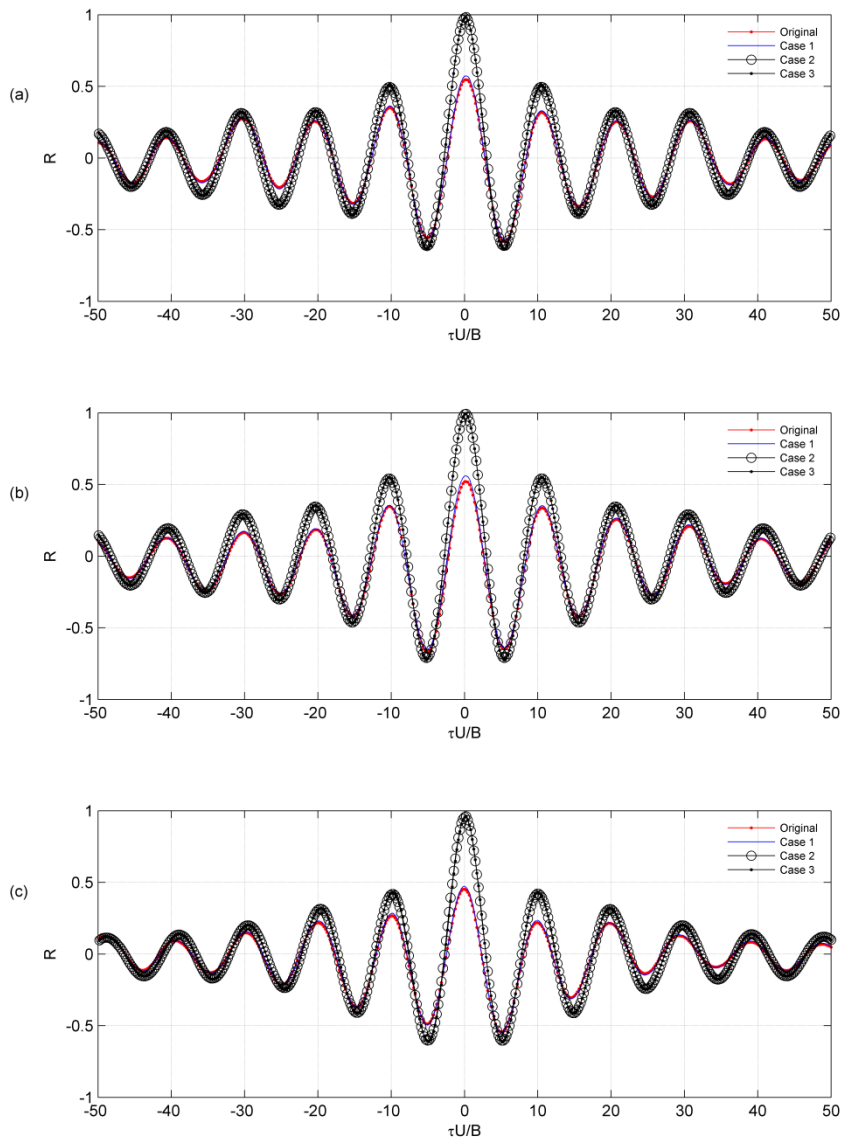


Fig. 11 Cross correlation between crosswind forces on the RSF and LSF, (a) Square tall building at wind incidence A; (b) H-section tall building at wind incidence A; (c) H-section tall building at wind incidence B. Original signals and reconstructed signals using first POD mode only by Case 1-3

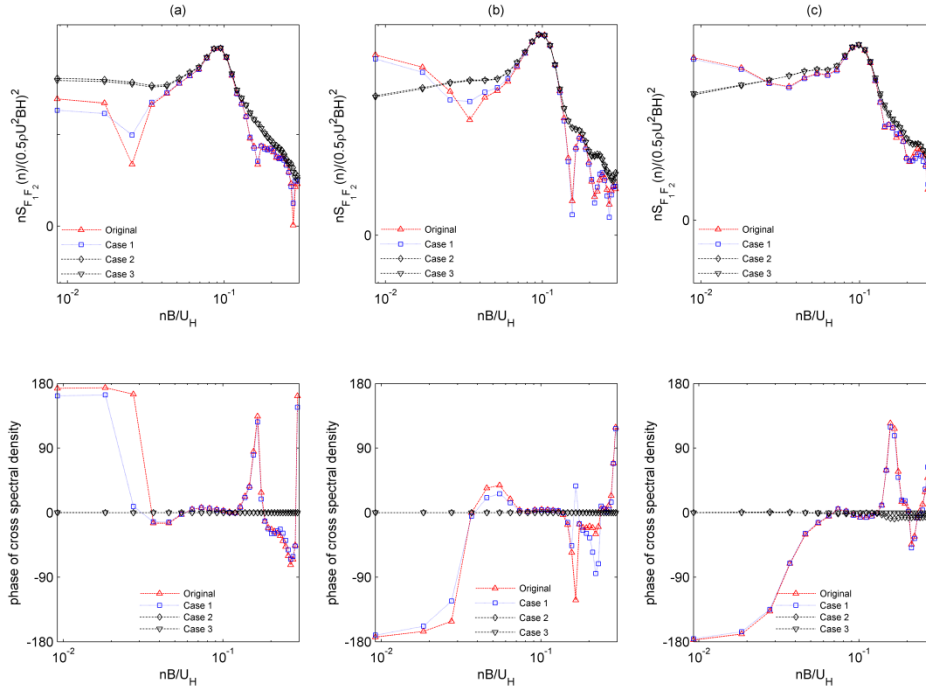


Fig. 12 Cross-power spectrum density and phase relationship of crosswind force coefficients on LSF and RSF, (a) Square tall building; (b) H-section tall building at wind incidence A; (c) H-section tall building at wind incidence B

5. Conclusions

This study has investigated the characteristics of fluctuating wind pressures on the side faces of a tall building, of $H/B = 6$, and their role in the generation of crosswind forces on the building with the space-time statistical tool of POD. A comparison is made on a square-section tall building and an H-section tall building to study the effect of recessed cavities, of size $W/B = D/B = 0.25$, on the modification of crosswind excitation.

The paper also compares the use of different pressure data sets for POD analysis in situations where pressures on two different surfaces are responsible for the generation of a wind force. The analysis makes use of the first POD mode and the crosswind force components reconstructed from this mode. It is found that while using the wind pressures on the two side faces separately lead to better representation of the individual side face crosswind forces, there are negligible differences in the net crosswind force signal in using different sets of data.

For the POD modes of wind pressures on the two side faces, the first 50 modes are required to contain over 90% of the total energy. However for the crosswind forces given by the spatial integration of wind pressures on a side face or both side faces, the use of the first POD mode alone can reconstruct the original force signal to a high accuracy, especially for the square tall building. This may support that the generation on crosswind forces on the building is largely contributed by

the global out-of-phase fluctuations of wind pressures on the two side faces in POD Mode 1 as a result of coherent vortex shedding from the building. The excellent reconstruction is revealed by the cross correlation relationship between the two side face crosswind forces. For the H-section tall building, the presence of the recessed cavities is found to result in a slight reduction of dominance of the first POD mode. This may explain the effect of the recessed cavities in reducing the overall crosswind excitation on the building.

It remains unresolved as regard to whether the pressure data sets of the windward and leeward surfaces should be included in the POD analysis. This issue needs further investigation.

Acknowledgments

This investigation was supported by a research grant awarded by the Research Grants Council of Hong Kong (HKU/713813).

References

- Armitt, J. (1968), "Eigenvector analysis of pressure fluctuations on the west instrumented cooling tower", *Internal Rep*, Central Electricity Research Laboratories, UK, 1968, RD/L/N114/68.
- Baker, C.J. (2000), "Aspects of the use of proper orthogonal decomposition of surface pressure fields", *Wind Struct.*, **3**(2), 97-115.
- Bartoli, G. and Ricciardelli, F. (2010), "Characterisation of pressure fluctuations on the leeward and side faces of rectangular buildings and accuracy of the quasi-steady loads", *J. Wind Eng. Ind. Aerod.*, **98**(10-11), 512-519.
- Best, R.J. and Holmes, J.D. (1983), "Use of eigenvalues in the covariance integration method for determination of wind load effects", *J. Wind Eng. Ind. Aerodyn.*, **13**(1-3), 359-370.
- Bienkiewicz, B., Ham, H.J. and Sun, Y. (1993), "Proper orthogonal decomposition of roof pressure", *J. Wind Eng. Ind. Aerod.*, **50**(C), 193-202.
- Bienkiewicz, B., Tamura, Y., Ham, H.J., Ueda, H. and Hibi, K. (1995), "Proper orthogonal decomposition and reconstruction of multi-channel roof pressure", *J. Wind Eng. Ind. Aerod.*, **54-55**(C), 369-381.
- Carassale, L. (2012), "Analysis of aerodynamic Interpretation of wind-induced pressure measurements by dynamic coherent structures fields by Independent Component Analysis", *Probabilist. Eng. Mech.*, **8**, 66-74.
- Carassale, L. and Brunenghi, M.M. (2011), "Statistical analysis of wind-induced pressure fields: A methodological perspective", *J. Wind Eng. Ind. Aerod.*, **99**(6-7), 700-710.
- Carassale, L., Solari, G. and Tubino, F. (2007), "Proper orthogonal decomposition in wind engineering. Part 2: Theoretical aspects and some applications", *Wind Struct.*, **10**(2), 177-208.
- Cheng, C.C.K., Lam, K.M., Leung, A.Y.T., Yang, K., Li, D.H.W. and Cheung, S.C.P. (2011), "Wind-induced natural ventilation of re-entrant bays in a high-rise building", *J. Wind Eng. Ind. Aerod.*, **99**(2-3), 79-90.
- Dutton, R. and Isyumov, N. (1990), "Reduction of tall building motion by aerodynamic treatments", *J. Wind Eng. Ind. Aerod.*, **36**(2), 739-747.
- Holmes, J. D. (2015), "Wind Loading of Structures", 3rd Ed., CRC Press, Boca Raton, Florida, USA.
- Holmes, J.D., Denoon, R., Kwok, K.C.S. and Glanville, M.J. (1997), "Wind loading and response of large stadium roofs", *Proceedings of the IASS International Symposium on Shell and Spatial Structures*, Singapore.
- Irwin, H.P.A.H., Cooper, K. and Girard, R. (1979), "Correction of distortion effects caused by tubing systems in measurements of fluctuating pressures", *J. Wind Eng. Ind. Aerod.*, **5**(1-2), 93-107.

- Jeong, S.H., Bienkiewicz, B. and Ham, H.J. (2000), "Proper orthogonal decomposition of building wind pressure specified at non-uniformly distributed pressure taps", *J. Wind Eng. Ind. Aerod.*, **87**(1), 1-14.
- Kareem, A. and Cermak, J.E. (1984), "Pressure fluctuations on a square building model in boundary-layer flows", *J. Wind Eng. Ind. Aerod.*, **16**(1), 17-41.
- Kim, Y.C. and Kanda, J. (2010), "Effects of taper and set-back on wind force and wind-induced response of tall buildings", *Wind Struct.*, **13**(6), 499-517.
- Kwok, K.C.S. (1988), "Effect of building shape on wind-induced response of tall buildings", *J. Wind Eng. Ind. Aerod.*, **28**(1-3), 381-390.
- Lam, K.M., Cheng, L., Zhao, J.G. and To, A.P. (2011), "Analysis of wind pressure relationship on two faces of a large cantilevered roof using proper orthogonal decomposition", *Proceedings of the 11th Int. Conf. Wind Engineering*, The Netherlands.
- Lee, B.E. (1975), "The effect of turbulence on the surface pressure field of a square prism", *J. Fluid Mech.*, **69**(2), 263-282.
- Sirovich, L. (1987), "Turbulence and the dynamics of coherent structures", *Q. Appl. Math.*, 561-571.
- Solari, G., Carassale, L. and Tubino, F. (2007), "Proper orthogonal decomposition in wind engineering. Part 1: A state-of-the-art and some prospects", *Wind Struct.*, **10**(2), 153-176.
- Tamura, Y. and Suganuma, S. (1999), "Proper orthogonal decomposition of random wind pressure field", *J. Fluid. Struct.*, **13**(7-8), 1069-1095.
- To, A.P., Lam, K.M. and Xie, Z.N. (2012), "Effect of a through-building gap on wind-induced loading and dynamic responses of a tall building", *Wind Struct.*, **15**(6), 531-553.
- Tse, K.T., Hitchcock, P.A., Kwok, K.C.S., Thepmongkorn, S. and Chan, C.M. (2009), "Economic perspectives of aerodynamic treatments of square tall buildings", *J. Wind Eng. Ind. Aerod.*, **97**(9-10), 455-467.
- Wong, S.Y. and K.M. Lam. (2013), "Effect of recessed cavities on wind-induced loading and dynamic responses of a tall building", *J. Wind Eng. Ind. Aerod.*, **114**, 72-82.